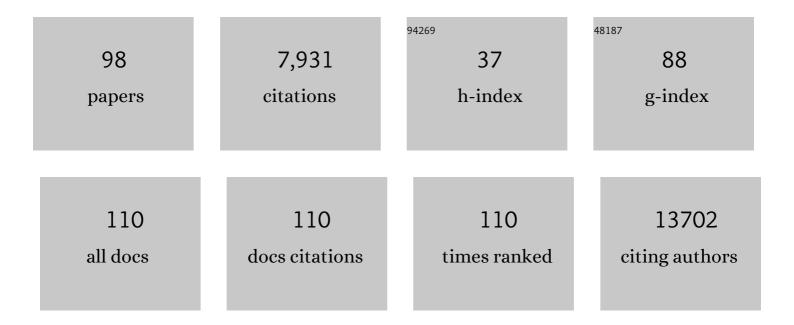
Robert G Palgrave

List of Publications by Year in descending order

Source: https://exaly.com/author-pdf/9346587/publications.pdf Version: 2024-02-01



#	Article	IF	CITATIONS
1	Band alignment of rutile and anatase TiO2. Nature Materials, 2013, 12, 798-801.	13.3	1,924
2	Self-cleaning coatings. Journal of Materials Chemistry, 2005, 15, 1689.	6.7	855
3	On the application of the tolerance factor to inorganic and hybrid halide perovskites: a revised system. Chemical Science, 2016, 7, 4548-4556.	3.7	757
4	Triazineâ€Based Graphitic Carbon Nitride: a Twoâ€Đimensional Semiconductor. Angewandte Chemie - International Edition, 2014, 53, 7450-7455.	7.2	523
5	Titania and silver–titania composite films on glass—potent antimicrobial coatings. Journal of Materials Chemistry, 2007, 17, 95-104.	6.7	304
6	Intelligent Multifunctional VO ₂ /SiO ₂ /TiO ₂ Coatings for Self-Cleaning, Energy-Saving Window Panels. Chemistry of Materials, 2016, 28, 1369-1376.	3.2	221
7	Atmospheric pressure chemical vapour deposition of SnSe and SnSe2 thin films on glass. Thin Solid Films, 2008, 516, 4750-4757.	0.8	156
8	Aerosol Assisted Chemical Vapor Deposition Using Nanoparticle Precursors:Â A Route to Nanocomposite Thin Films. Journal of the American Chemical Society, 2006, 128, 1587-1597.	6.6	151
9	Visible Light Photo-oxidation of Model Pollutants Using CaCu ₃ Ti ₄ O ₁₂ : An Experimental and Theoretical Study of Optical Properties, Electronic Structure, and Selectivity. Journal of the American Chemical Society, 2011, 133, 1016-1032.	6.6	130
10	Evidence and Effect of Photogenerated Charge Transfer for Enhanced Photocatalysis in WO ₃ /TiO ₂ Heterojunction Films: A Computational and Experimental Study. Advanced Functional Materials, 2017, 27, 1605413.	7.8	115
11	Concurrent Photocatalytic Hydrogen Generation and Dye Degradation Using MILâ€125â€NH ₂ under Visible Light Irradiation. Advanced Functional Materials, 2018, 28, 1806368.	7.8	110
12	Elucidating the deprotonation of polyaniline films by X-ray photoelectron spectroscopy. Journal of Materials Chemistry C, 2015, 3, 7180-7186.	2.7	95
13	Anion Distribution, Structural Distortion, and Symmetry-Driven Optical Band Gap Bowing in Mixed Halide Cs ₂ SnX ₆ Vacancy Ordered Double Perovskites. Chemistry of Materials, 2019, 31, 9430-9444.	3.2	83
14	Aerosol assisted chemical vapour deposition of photochromic tungsten oxide and doped tungsten oxide thin films. Journal of Materials Chemistry, 2004, 14, 2864.	6.7	79
15	Probing the chemical structure of monolayer covalent-organic frameworks grown via Schiff-base condensation reactions. Chemical Communications, 2016, 52, 9941-9944.	2.2	78
16	Application of high resolution DLP stereolithography for fabrication of tricalcium phosphate scaffolds for bone regeneration. Biomedical Materials (Bristol), 2019, 14, 045018.	1.7	78
17	Scalable route to CH ₃ NH ₃ PbI ₃ perovskite thin films by aerosol assisted chemical vapour deposition. Journal of Materials Chemistry A, 2015, 3, 9071-9073.	5.2	75
18	A Polar Corundum Oxide Displaying Weak Ferromagnetism at Room Temperature. Journal of the American Chemical Society, 2012, 134, 3737-3747.	6.6	73

#	Article	IF	CITATIONS
19	Engineering Valence Band Dispersion for High Mobility p-Type Semiconductors. Chemistry of Materials, 2017, 29, 2402-2413.	3.2	66
20	Bandgap lowering in mixed alloys of Cs ₂ Ag(Sb _x Bi _{1â^'x})Br ₆ double perovskite thin films. Journal of Materials Chemistry A, 2020, 8, 21780-21788.	5.2	66
21	Aerosol assisted chemical vapour deposition of WO3 thin films from tungsten hexacarbonyl and their gas sensing properties. Journal of Materials Chemistry, 2007, 17, 3708.	6.7	64
22	Nitrogen diffusion in doped TiO2 (110) single crystals: a combined XPS and SIMS study. Journal of Materials Chemistry, 2009, 19, 8418.	6.7	64
23	Aerosol Assisted Chemical Vapor Deposition of Gold and Nanocomposite Thin Films from Hydrogen Tetrachloroaurate(III). Chemistry of Materials, 2007, 19, 4639-4647.	3.2	63
24	Nucleobase pairing and photodimerization in a biologically derived metal-organic framework nanoreactor. Nature Communications, 2019, 10, 1612.	5.8	58
25	Aerosol-assisted chemical vapour deposition of WO3 thin films using polyoxometallate precursors and their gas sensing properties. Journal of Materials Chemistry, 2007, 17, 1063.	6.7	57
26	Optimized Atmospheric-Pressure Chemical Vapor Deposition Thermochromic VO ₂ Thin Films for <i>Intelligent</i> Window Applications. ACS Omega, 2017, 2, 1040-1046.	1.6	56
27	Electronic and Structural Properties of Sn _{<i>x</i>} Ti _{1â^'<i>x</i>} O ₂ (0.0 ≤i>x≤0.1) Solid Solutions. Chemistry of Materials, 2010, 22, 1551-1558.	3.2	55
28	Atmospheric Pressure CVD of Molybdenum Diselenide Films on Glass. Chemical Vapor Deposition, 2006, 12, 692-698.	1.4	53
29	A critical evaluation of the mode of incorporation of nitrogen in doped anatase photocatalysts. Physical Chemistry Chemical Physics, 2010, 12, 960-969.	1.3	52
30	Indium Gallium Oxide Alloys: Electronic Structure, Optical Gap, Surface Space Charge, and Chemical Trends within Common-Cation Semiconductors. ACS Applied Materials & Interfaces, 2021, 13, 2807-2819.	4.0	50
31	Electronic basis of visible region activity in high area Sn-doped rutile TiO2 photocatalysts. Physical Chemistry Chemical Physics, 2011, 13, 7882.	1.3	49
32	A Nature-Inspired Conjugated Polymer for High Performance Transistors and Solar Cells. Macromolecules, 2015, 48, 5148-5154.	2.2	48
33	Aerosol-assisted chemical vapor deposition of V2O5 cathodes with high rate capabilities for magnesium-ion batteries. Journal of Power Sources, 2018, 384, 355-359.	4.0	48
34	Gallium oxide thin films from the AACVD of [Ga(NMe2)3]2 and donor functionalised alcohols. Dalton Transactions, 2008, , 591.	1.6	44
35	An assessment of silver copper sulfides for photovoltaic applications: theoretical and experimental insights. Journal of Materials Chemistry A, 2016, 4, 12648-12657.	5.2	42
36	Advanced XPS characterization: XPS-based multi-technique analyses for comprehensive understanding of functional materials. Materials Chemistry Frontiers, 2021, 5, 7931-7963.	3.2	41

#	Article	IF	CITATIONS
37	Enhancing tissue integration and angiogenesis of a novel nanocomposite polymer using plasma surface polymerisation, an in vitro and in vivo study. Biomaterials Science, 2016, 4, 145-158.	2.6	37
38	Syntheses, X-ray structures and CVD studies of diorganoalkoxogallanes. Journal of Organometallic Chemistry, 2008, 693, 1787-1796.	0.8	36
39	Modular and Versatile Spatial Functionalization of Tissue Engineering Scaffolds through Fiberâ€Initiated Controlled Radical Polymerization. Advanced Functional Materials, 2015, 25, 5748-5757.	7.8	35
40	Argon plasma improves the tissue integration and angiogenesis of subcutaneous implants by modifying surface chemistry and topography. International Journal of Nanomedicine, 2018, Volume 13, 6123-6141.	3.3	35
41	Geometric Analysis and Formability of the Cubic A ₂ BX ₆ Vacancy-Ordered Double Perovskite Structure. Chemistry of Materials, 2020, 32, 9573-9583.	3.2	35
42	Bioinspired Polymerization of Quercetin to Produce a Curcumin-Loaded Nanomedicine with Potent Cytotoxicity and Cancer-Targeting Potential in Vivo. ACS Biomaterials Science and Engineering, 2019, 5, 6036-6045.	2.6	34
43	Hybrid Organic–Inorganic Coordination Complexes as Tunable Optical Response Materials. Inorganic Chemistry, 2016, 55, 3393-3400.	1.9	31
44	Chemical vapour deposition of titanium chalcogenides and pnictides and tungsten oxide thin films. New Journal of Chemistry, 2006, 30, 505.	1.4	30
45	Artificial Construction of the Layered Ruddlesden–Popper Manganite La ₂ Sr ₂ Mn ₃ O ₁₀ by Reflection High Energy Electron Diffraction Monitored Pulsed Laser Deposition. Journal of the American Chemical Society, 2012, 134, 7700-7714.	6.6	29
46	â€~Sticky electrodes' for the detection of silver nanoparticles. Nanotechnology, 2013, 24, 295502.	1.3	28
47	Surfactant directed chemical vapour deposition of gold nanoparticles with narrow size distributions. Gold Bulletin, 2008, 41, 66-69.	3.2	27
48	Spatial Electron-hole Separation in a One Dimensional Hybrid Organic–Inorganic Lead Iodide. Scientific Reports, 2016, 6, 20626.	1.6	25
49	Development of mechano-responsive polymeric scaffolds using functionalized silica nano-fillers for the control of cellular functions. Nanomedicine: Nanotechnology, Biology, and Medicine, 2016, 12, 1725-1733.	1.7	25
50	Correlation of Optical Properties, Electronic Structure, and Photocatalytic Activity in Nanostructured Tungsten Oxide. Advanced Materials Interfaces, 2017, 4, 1700064.	1.9	25
51	An experimental and theoretical study into NaSbS ₂ as an emerging solar absorber. Journal of Materials Chemistry C, 2019, 7, 2059-2067.	2.7	25
52	Phase quantification by X-ray photoemission valence band analysis applied to mixed phase TiO2 powders. Applied Surface Science, 2017, 423, 205-209.	3.1	24
53	Experimental validation of calculated atomic charges in ionic liquids. Journal of Chemical Physics, 2018, 148, 193817.	1.2	24
54	A solution chemistry approach to epitaxial growth and stabilisation of Bi ₂ Ti ₂ O ₇ films. Journal of Materials Chemistry A, 2014, 2, 18241-18245.	5.2	23

#	Article	IF	CITATIONS
55	Accelerated optimization of transparent, amorphous zinc-tin-oxide thin films for optoelectronic applications. APL Materials, 2019, 7, .	2.2	23
56	Qualitative XANES and XPS Analysis of Substrate Effects in VO ₂ Thin Films: A Route to Improving Chemical Vapor Deposition Synthetic Methods?. Journal of Physical Chemistry C, 2017, 121, 20345-20352.	1.5	22
57	Shedding Light on the Protonation States and Location of Protonated N Atoms of Adenine in Metal–Organic Frameworks. Inorganic Chemistry, 2018, 57, 1888-1900.	1.9	21
58	Enhanced visible light absorption in layered Cs ₃ Bi ₂ Br ₉ through mixed-valence Sn(<scp>ii</scp>)/Sn(<scp>iv</scp>) doping. Chemical Science, 2021, 12, 14686-14699.	3.7	21
59	Interfacial Diffusion during Growth of SnO ₂ (110) on TiO ₂ (110) by Oxygen Plasma Assisted Molecular Beam Epitaxy. Crystal Growth and Design, 2009, 9, 1793-1797.	1.4	20
60	A fast and effective method for N-doping TiO2 by post treatment with liquid ammonia: visible light photocatalysis. Thin Solid Films, 2014, 562, 223-228.	0.8	20
61	Plasma Surface Modification of Polyhedral Oligomeric Silsequioxane-Poly(carbonate-urea) Urethane with Allylamine Enhances the Response and Osteogenic Differentiation of Adipose-Derived Stem Cells. ACS Applied Materials & Interfaces, 2016, 8, 18701-18709.	4.0	20
62	Nanoscale, conformal films of graphitic carbon nitride deposited at room temperature: a method for construction of heterojunction devices. Nanoscale, 2017, 9, 16586-16590.	2.8	20
63	Atomic charges of sulfur in ionic liquids: experiments and calculations. Faraday Discussions, 2017, 206, 183-201.	1.6	20
64	Preparation and characterisation of high-density ionic liquids incorporating halobismuthate anions. Dalton Transactions, 2014, 43, 10910-10919.	1.6	19
65	The strong catalytic effect of Pb(ii) on the oxygen reduction reaction on 5 nm gold nanoparticles. Physical Chemistry Chemical Physics, 2014, 16, 3200.	1.3	19
66	Emerging Earth-Abundant Solar Absorbers. ACS Energy Letters, 2022, 7, 1553-1557.	8.8	19
67	Rutile to anatase phase transition induced by N doping in highly oriented TiO ₂ films. Physical Chemistry Chemical Physics, 2016, 18, 24722-24728.	1.3	17
68	NEXAFS spectroscopy of ionic liquids: experiments <i>versus</i> calculations. Physical Chemistry Chemical Physics, 2017, 19, 31156-31167.	1.3	16
69	Demonstration of Visible Light-Activated Photocatalytic Self-Cleaning by Thin Films of Perovskite Tantalum and Niobium Oxynitrides. ACS Applied Materials & Interfaces, 2020, 12, 33603-33612.	4.0	16
70	Reactivity of ZrCl4 and HfCl4 with silylamines and thermal decomposition of the compounds [MCl4{NH(R)(SiR′3)}] (M=Zr, Hf, R=tBu, R′=Me; R=SiR′3=SiMe3, SiMe2H). Polyhedron, 2008, 27, 1041-	1048.	15
71	Singlet Oxygen and the Origin of Oxygen Functionalities on the Surface of Carbon Electrodes. Angewandte Chemie - International Edition, 2018, 57, 6270-6273.	7.2	15
72	Direct and continuous hydrothermal flow synthesis of thermochromic phase pure monoclinic VO ₂ nanoparticles. Journal of Materials Chemistry C, 2018, 6, 11731-11739.	2.7	15

#	Article	IF	CITATIONS
73	Patterning of metal oxide thin films using a H ₂ /He atmospheric pressure plasma jet. Green Chemistry, 2020, 22, 1406-1413.	4.6	15
74	Nitridation of nanocrystalline TiO2 thin films by treatment with ammonia. Thin Solid Films, 2011, 519, 3587-3595.	0.8	14
75	BaBi ₂ O ₆ : A Promising n-Type Thermoelectric Oxide with the PbSb ₂ O ₆ Crystal Structure. Chemistry of Materials, 2021, 33, 7441-7456.	3.2	11
76	Singlet Oxygen and the Origin of Oxygen Functionalities on the Surface of Carbon Electrodes. Angewandte Chemie, 2018, 130, 6378-6381.	1.6	10
77	Synthesis, structural analysis, electrochemical and magnetic properties of tetrachloroferrate ionic liquids. New Journal of Chemistry, 2021, 45, 13429-13440.	1.4	10
78	Order of magnitude increase in photocatalytic rate for hierarchically porous anatase thin films synthesized from zinc titanate coatings. Dalton Transactions, 2017, 46, 1975-1985.	1.6	9
79	Electron spectroscopy of ionic liquids: experimental identification of atomic orbital contributions to valence electronic structure. Physical Chemistry Chemical Physics, 2019, 21, 18893-18910.	1.3	9
80	Degradation of Layered Oxide Cathode in a Sodium Battery: A Detailed Investigation by Xâ€Ray Tomography at the Nanoscale. Small Methods, 2021, 5, e2100596.	4.6	9
81	Solvothermal water-diethylene glycol synthesis of LiCoPO ₄ and effects of surface treatments on lithium battery performance. RSC Advances, 2019, 9, 740-752.	1.7	8
82	Synthesis and Charaterisation of Chromium Oxyselenide (Cr2Se0.7O2.3) Formed from Chemical Vapour Synthesis: A New Antiferromagnet. European Journal of Inorganic Chemistry, 2007, 2007, 4579-4582.	1.0	7
83	Gas-sensing properties of Fe2â^'xTixO3+γ (x=0–1.4). Polyhedron, 2010, 29, 1225-1230.	1.0	7
84	Dualâ€Functional Photocatalysis: Concurrent Photocatalytic Hydrogen Generation and Dye Degradation Using MILâ€125â€NH ₂ under Visible Light Irradiation (Adv. Funct. Mater. 52/2018). Advanced Functional Materials, 2018, 28, 1870373.	7.8	6
85	Experimental measurement and prediction of ionic liquid ionisation energies. Physical Chemistry Chemical Physics, 2021, 23, 20957-20973.	1.3	6
86	LaSrCo _{0.5} Rh _{0.5} O _{3.25} and LaSrNi _{0.5} Rh _{0.5} O _{3.25} :Topochemically Reduced, Mixed Valence Rh(I)/Rh(III) Oxides. Inorganic Chemistry, 2020, 59, 13767-13773.	1.9	4
87	Bifunctional redox tagging of carbon nanoparticles. Nanoscale, 2015, 7, 2069-2075.	2.8	3
88	An X-ray photoelectron spectroscopy study of ionic liquids based on a bridged dicationic moiety. Journal of Chemical Research, 2022, 46, 174751982210929.	0.6	3
89	Resonant Electron Spectroscopy: Identification of Atomic Contributions to Valence States. Faraday Discussions, 2022, , .	1.6	2
90	Photocatalysis: Evidence and Effect of Photogenerated Charge Transfer for Enhanced Photocatalysis in WO ₃ /TiO ₂ Heterojunction Films: A Computational and Experimental Study (Adv. Funct. Mater. 18/2017). Advanced Functional Materials, 2017, 27, .	7.8	1

#	Article	IF	CITATIONS
91	Quantifying the Polymeric Capping of Nanoparticles with Xâ€Ray Photoelectron Spectroscopy. ChemPhysChem, 2018, 19, 1341-1343.	1.0	1
92	Electroâ€Oxidation of Titanium Carbide Nanoparticles in Aqueous Acid Creates TiC@TiO 2 Coreâ€Shell Structures. ChemElectroChem, 2021, 8, 911-917.	1.7	1
93	Multicoated composites of nano silicon and graphene nanoplatelets as anodes in Li-ion batteries. Materials Advances, 0, , .	2.6	1
94	Chapter 10. CVD of Functional Coatings on Glass. , 0, , 451-476.		0
95	Frontispiece: Triazine-Based Graphitic Carbon Nitride: a Two-Dimensional Semiconductor. Angewandte Chemie - International Edition, 2014, 53, n/a-n/a.	7.2	0
96	Frontispiz: Triazine-Based Graphitic Carbon Nitride: a Two-Dimensional Semiconductor. Angewandte Chemie, 2014, 126, n/a-n/a.	1.6	0
97	Controlled Polymerization: Modular and Versatile Spatial Functionalization of Tissue Engineering Scaffolds through Fiberâ€Initiated Controlled Radical Polymerization (Adv. Funct. Mater. 36/2015). Advanced Functional Materials, 2015, 25, 5718-5718.	7.8	0
98	Structure and magnetism of the Rh4+-containing perovskite oxides La0.5Sr0.5Mn0.5Rh0.5O3 and La0.5Sr0.5Fe0.5Rh0.5O3. Dalton Transactions, 2020, 49, 11346-11353.	1.6	0